Maejo Int. J. Sci. Technol. **2015**, *9*(02), 165-180

Maejo International Journal of Science and Technology

ISSN 1905-7873

Available online at www.mijst.mju.ac.th

Full Paper

Defining the soil parameters for computing deformations caused by braced excavation

Linlong Mu [1, 2, 3, *], Richard J. Finno [3], Maosong Huang [1, 2], Taesik Kim [4] and Kristi Kern [3]

[1] Department of Geotechnical Engineering, Tongji University, Shanghai, 200092, China

[2] Key Laboratory of Geotechnical and Underground Engineering of Ministry of Education, Tongji University, Shanghai, 200092, China

[3] Department of Civil and Environment Engineering, Northwestern University, Evanston, IL, 60201, USA

[4] Department of Civil Engineering, Hongik University, Seoul, Korea

[*] Corresponding author, e-mail: mulinlong@tongji.edu.cn

Received: 31 March 2014 / Accepted: 22 June 2015 / Published: 26 June 2015

Abstract: Evaluation of the soil response is required to estimate the potential building damage caused by excavations. Using proper soil parameters is a key ingredient when computing soil responses, assuming the model represents the actual soil response in a reasonable way. Soil parameters are usually identified from laboratory experiments performed on tube samples or from *in situ* tests, but large uncertainties are associated with these methods for most projects. Inverse analysis is a quantitative technique that allows one to select parameters to fit the responses of soil from both laboratory tests and field observations. The technique is applied to results of both the laboratory experiments on block and thin-walled tube samples and the field performance data, all of which were collected from an excavation made through Chicago clays. The results of computed soil responses based on the hardening soil (HS) model and the hardening soil with small strain (HSS) model found in the computer code Plaxis are compared to illustrate the problems that are likely to be encountered in practical application of finite element simulations. Guidance is provided for selecting the parameters from laboratory tests to compute the field responses for braced excavation loadings.

Keywords: braced excavation, soil parameters, finite element, small strain, stress probing test

Maejo Int. J. Sci. Technol. **2015**, *9*(02), 165-180

INTRODUCTOIN

Many projects in geotechnical practice require a relatively accurate computation of ground deformations. For example, ground deformations are required when evaluating the damage potential arising from construction-induced deformations of structures and utilities surrounding deep supported excavations. It is generally recognised that the modelling of soil behaviour at small strain levels is required to estimate the excavation-induced ground settlement adjacent to excavations [1-5]. In many urban areas, buildings adjacent to excavations are supported by deep foundations. To estimate the potential damage to these foundations, it is also important to estimate soil movements below the ground surface. Considering the complex conditions around excavations, the finite element method (FEM) is commonly used to compute wall deflections and the distribution of ground movements. The use of an appropriate soil model and attendant parameters are the key ingredients for computing soil responses in these situations. Laboratory experiments are commonly used to select the soil parameters for design, but they are affected by sample quality and details of experiments, especially when the strain is small. Because of these inherent uncertainties, it is useful to understand the relationship between parameters based on both laboratory experiments and field observations.

The soil around an excavation is subjected to a variety of stress paths [6-8]. In general, the soil in front of a retaining wall is subjected to extension, whereas the soil behind a retaining wall is subjected to reduced compression. While it is the goal of a well-formulated constitutive model to represent the soil behaviour for all loading paths, this is rarely realised in practice. For a given soil model, the parameters based on laboratory experiments for these paths may differ, and these in turn may differ from those found from the best fit of various aspects of field performance data. Thus, it is useful to evaluate the difference in soil parameters based on these types of data, particularly in terms of models commonly used in practice. However, the inverse analysis is currently only used to calibrate the soil parameters of a soil model that did not consider the small strain behaviour based on field performance data.

In this paper inverse analysis is used to identify soil parameters for the hardening soil (HS) model and the hardening soil with small strain (HSS) model based on triaxial test results on specimens cut from thin-walled tube and block samples and on field performance data from the excavation at the Block 37 project in Chicago, IL, USA. The Block 37 project was a top-down construction project completed in an urban environment. The excavation commenced in 2007 and was completed in 2008. The models were chosen because they are found in a commonly used commercial finite element code and represent current practice in many areas. The relationship between the soil stiffness obtained from laboratory experiments and field observations is discussed in light of the different stress paths and strain levels aimed at defining the triaxial stress test most suited to calibrate the soil parameters that are most relevant to the simulation of an excavation system while considering the small strain behaviour of the soil.

PROCEDURE

Inverse Analysis

Inverse analysis techniques have been applied to geotechnical engineering problems and found to be useful for quantifying parameters and updating performance computations [9-11]. Herein, inverse

analyses were used to find proper stiffness parameters for the HSS and HS models based on both triaxial test data and lateral movements measured during excavation. The inverse analysis based on a gradient method was conducted by coupling the optimisation toolbox in the mathematical code Matlab with the finite element code Plaxis 9.0. Because Plaxis is a closed program, we can only input and output the data through the interface of the program. A macro program was written to read the calibration results from Matlab, which were then written into Plaxis through the interface of Plaxis. Next, the analysis results of the Plaxis program, which were subsequently written into Matlab, were also read by the macro program through the interface of Plaxis. The method used to find the best fit between the computed and observed values is defined by a weighted least-square objective function, F(**b**):

$$F(\mathbf{b}) = [\mathbf{y} - \mathbf{y}'(\mathbf{b})]^T \boldsymbol{\omega} [\mathbf{y} - \mathbf{y}'(\mathbf{b})] \quad (1)$$

where **b** is a vector containing values of the number of parameters to be estimated, **y** is the vector of the observations being matched by the regression, $\mathbf{y}'(\mathbf{b})$ is the vector of the computed values that correspond to the observations and $\boldsymbol{\omega}$ is the weight matrix. As Calvello [11] described, the weighting is used to reduce the influence of observations that are less reliable and increase the influence of observations that are more reliable. In this work a diagonal weight matrix is used. The weight of every observation, ω_{ii}, is equal to the inverse of its error variance $\omega_{ii} = \frac{1}{\sigma_i^2}$. When analysing the triaxial test results, the standard deviation, σ_i, is

$$\sigma_i = \frac{\varepsilon_i}{1.96} \quad (2)$$

where ε_i is the measurement error of the observations (stress, pore pressure and volumetric strain) in the laboratory tests. In the excavation analysis using inclinometer data as observations, $\sigma_i = 0.0001 d_i$, where d_i is the distance from the bottom of the inclinometer casing.

The objective function values F(b) quantitatively describe how well the computed results based on the optimised parameters fit the test results. A lower F(b) value indicates a better fit.

Soil Model

The behaviour of the HSS model is determined by 13 parameters: ϕ (friction angle), c (cohesion), R_f(failure ratio), Ψ (dilatancy angle), v_{ur} (Poisson's ratio), K_0 (static earth pressure coefficient at rest), OCR (over-consolidation ratio), E_{50}^{ref} (secant stiffness in standard drained triaxial test), E_{oed}^{ref} (tangent stiffness for primary odometer loading), E_{ur}^{ref} (unloading-reloading stiffness), m (power for stress-level dependency of stiffness), G_0^{ref} (reference shear modulus at very small strains) and $\gamma_{0.7}$ (shear strain at which the secant shear modulus is equal to $0.772G_0$). The details of the parameters and model formulation are described by Schanz et al.[12] and Benz et al. [13]. Note that G_0^{ref} and $\gamma_{0.7}$ are added to define the small strain behaviour [13] and other eleven parameters are the same as those used to define the behaviour according to the HS model [12].

Of the 13 parameters, ϕ, c and R_f are the Mohr-Coulomb failure criteria parameters [12, 14]. The stiffness of the soil is determined in the HSS model by E_{50}^{ref}, E_{oed}^{ref}, E_{ur}^{ref}, m, G_0^{ref} and $\gamma_{0.7}$. E_{oed}^{ref}

Maejo Int. J. Sci. Technol. **2015**, *9*(02), 165-180

and E_{ur}^{ref} are computed as 0.7 and 3 times E_{50}^{ref} respectively. The dilatancy angle, Ψ, is individually defined in the HS and HSS models. Although the dilatancy angle is usually zero for normal to lightly over-consolidated soil, it is optimised herein as a check. G_0^{ref} can be computed as follows:

$$G_0^{ref} = G_0\left(\frac{c\cos\phi - \sigma'_3 \sin\phi}{c\cos\phi + p^{ref}\sin\phi}\right)^{-m} \quad (3)$$

where σ'_3 is the horizontal effective stress, p^{ref} is the reference stress and G_0 is shear modulus at very small strains that can be computed by:

$$G_0 = \rho v^2 \quad (4)$$

where ρ is the density of the soil and v is shear wave propagation velocity through soil medium. This velocity can be evaluated from bender element tests in the laboratory. A bender element consists of two piezoceramic plates bonded together in parallel with a brass electrode plate in between. They are typically mounted on the base and top of the soil specimen as miniature cantilever beams. When excited by an input voltage, the source bender element bends, emitting a shear wave which travels through the soil specimen at shear wave velocity. The wave motion causes the receiver element to mechanically vibrate, which results in a voltage signal that is captured by a high-speed digital acquisition system. The shear wave velocity is calculated by determining the travel time of the shear wave between the tips of the source and receiver elements. In the field this velocity can be obtained by performing seismic cone penetration test (SCPT) that is equipped with a velocity geophone to measure shear wave propagation velocity. Both the bender element tests and SCPT were conducted to evaluate the shear wave propagation velocity at the site. The details of the tests were described by Kim [15].

One cannot use the inverse analysis to simultaneously compute the soil responses by optimising all 13 parameters. Thus, it is necessary to judiciously select the parameters to be optimised. As Calvello and Finno [16] showed for the HS model, the failure parameter, ϕ, and the stiffness parameters, m and E_{50}^{ref}, have the most impact on the computed values of lateral deformations measured close to a support wall of an excavation, based on the values of composite-scaled sensitivity. They also noted that m and E_{50}^{ref} are highly correlated parameters, and because one cannot simultaneously optimise parameters that have high correlation, E_{50}^{ref} was selected for optimisation because it is directly proportional to the soil stiffness. Details can be found in the work of Calvello and Finno [16]. Because this paper considers an excavation with relatively small deformations, which is a very practical application, the failure parameters were not optimised in the inverse analysis presented herein.

As seen in Figure 1, the shear wave velocities based on bender element tests on block samples reconsolidated against the *in situ* vertical effective stress with a 36-hour period of drained creep agree reasonably well with the shear wave velocities measured in the field using SCPT. (Detailed results of the tests can be found in Kim's work [15].) As such, G_0^{ref} is relatively well-defined in the laboratory and *in situ* for these clays and can be used to represent the maximum stiffness of the soil. Herein, the value of G_0^{ref} calculated from the bender element test results was used in the inverse analysis. Thus, three individual parameters, E_{50}^{ref}, Ψ and $\gamma_{0.7}$, were chosen for optimisation based on the triaxial test results. The remaining parameters were set to reasonable values based on site-specific data and parameters

Maejo Int. J. Sci. Technol. **2015**, *9*(02), 165-180

obtained from the inverse analysis of the Chicago State excavation project [11].

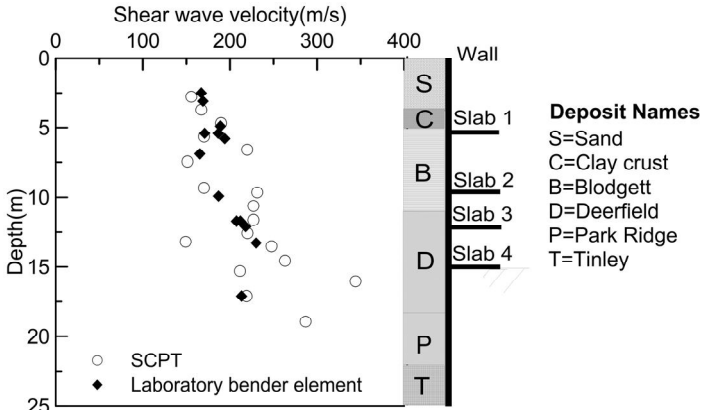

Figure 1. Measured shear wave velocity based on SCPT and bender element tests

CASE STUDY

Block 37 Project

The case study analysed herein is the Block 37 project located in downtown Chicago [17]. The excavation was approximately 110 m long and 110 m wide and was made through compressible soft-to-medium-stiff glacial clay to a depth of 15 m using a partial top-down construction technique. An existing freight tunnel was approximately 3 m away from the excavation near the retaining wall. A reinforced concrete-slurry wall and four concrete slabs were installed to laterally support the excavation.

The subsurface soil profile of Block 37 is shown in Figure 2. The geology and typical geotechnical characteristics of these deposits were presented by Finno and Chung [18]. The groundwater level was at a depth of 4 m below ground surface. The interior of the excavation was potholed to remove the old shallow foundations and then refilled prior to excavation. Inclinometers were installed around the perimeter to record the slurry wall and the soil movements behind the wall, as shown in Figure 3.

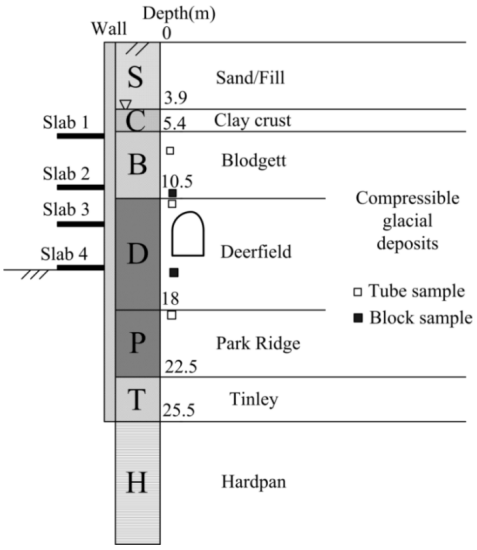

Figure 2. Soil profile of Block 37

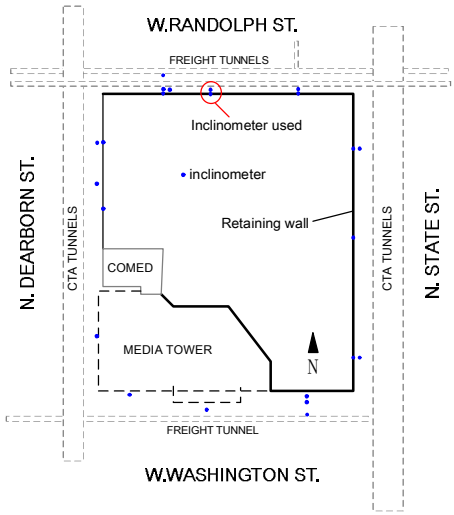

Figure 3. Inclinometer locations around Block 37

Maejo Int. J. Sci. Technol. **2015**, *9*(02), 165-180

Triaxial Testing Program

Thin-walled, 71-mm-diameter tube samples and hand-cut block samples were obtained from the compressible glacial deposits at the site at the depths shown in Figure 2. Triaxial experiments were conducted at Northwestern University using specimens cut from the tube samples and block samples. Complete details of the experimental program can be found in the work of Kim [15]. The specimens were K_0-consolidated to *in situ* stresses and then subjected to an approximately 36-hr drained creep period under constant effective stress until the axial strain was less than 0.001%/hr. Thereafter, the specimens were sheared along one of the stress paths in Figure 4, which shows a plot of the mean effective stress, p', against the deviator stress, q, with p' and q defined as:

$$p' = (\sigma'_a + 2\sigma'_r)/3 \quad (5)$$

$$q = \sigma'_a - \sigma'_r \quad (6)$$

where σ'_a is the effective axial stress and σ'_r is the effective radial stress. From Figure 4, undrained TC and RTE tests were conducted on both the specimens from tube samples and those cut from blocks, while drained CMS, CMSE and CQU tests were conducted on specimens cut from blocks.

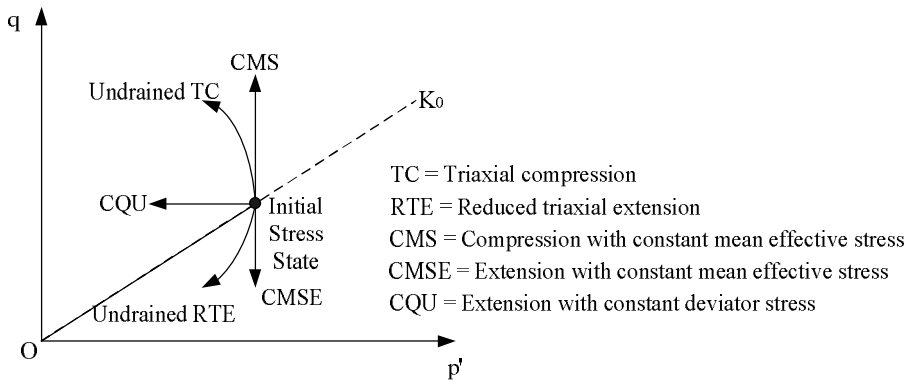

Figure 4. Stress probing paths of laboratorial triaxial tests

The internal deformations were measured using a pair of subminiature linear variable differential transformers mounted on the side of the specimen with a spring-loaded caliper placed around the centre of the specimen. The internal measurement system could resolve as small as 0.002% of axial strains, which is approximately the lower limit of small strain behaviour, as defined by Atkinson et al. [19]. Bender elements were incorporated into the system to allow the determination of G_0, as noted previously.

Figure 5 summarises the stress-strain responses obtained from the triaxial tests of samples from all three strata. These results form the basis of the laboratory observations used to quantitatively optimise the soil parameters. Both drained and undrained results are shown. The specimens were cut from blocks obtained in the softer Blodgett and Deerfield strata. Thin-walled tube samples were obtained from all three strata. The data plotted at this scale illustrate that the block specimens yielded stiffer and stronger responses than that of the tube specimens.

Maejo Int. J. Sci. Technol. **2015**, *9*(02), 165-180

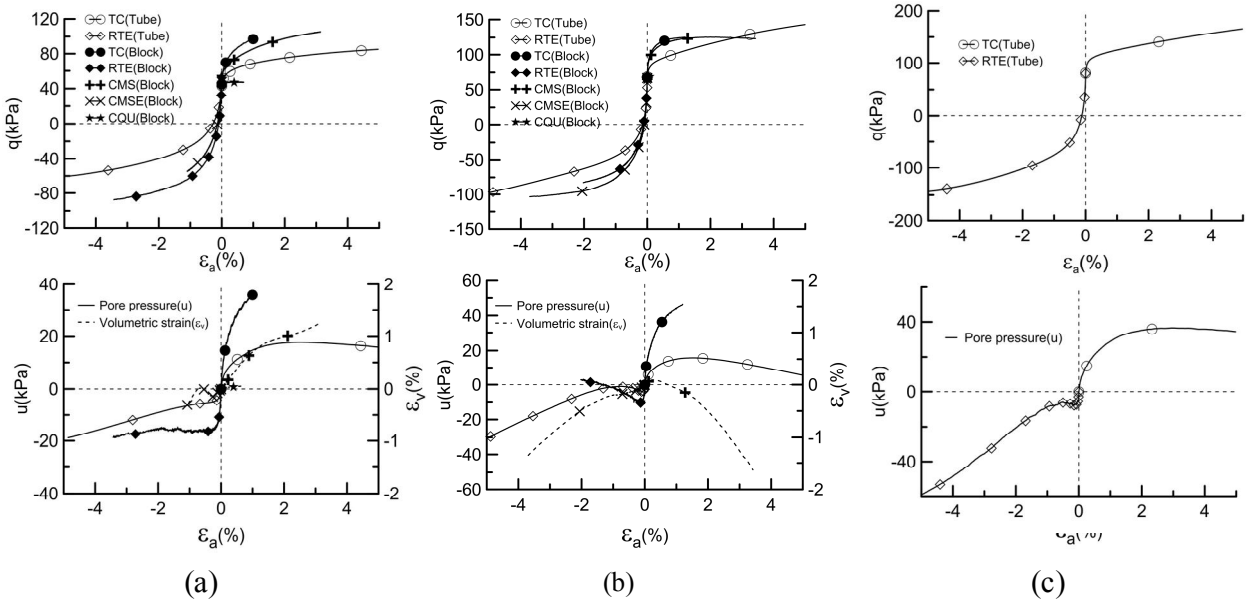

Figure 5. Results of triaxial tests: (a) Blodgett; (b) Deerfield; (c) Park Ridge

Observed Lateral Deformation Adjacent to Block 37 Excavation

The excavation process at Block 37 project was divided into five stages, as summarised in Table 1. The data from an inclinometer located 1 m behind the wall were typical of the responses during the excavation and were used as observations for the inverse analysis. This inclinometer was located near the centre of the north wall of the excavation where essentially no end restraints existed. Hence the behaviour at this location was plane strain and was simulated as such. Figure 6 shows the lateral ground deformations that developed immediately behind the wall during the excavation. As seen from the results, it is important to consider potholing in the simulation of the excavation because as much as 10 mm of wall deformation was induced by the potholing and refilling. Most of the subsequent deformations occurred during the first stage, when a 6.2-m cut was made prior to the placing of any lateral support.

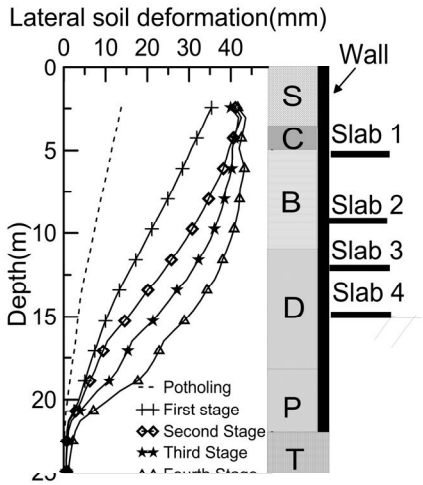

Figure 6. Measured lateral deformations of the soil 1 m behind the wall

Maejo Int. J. Sci. Technol. **2015**, *9*(02), 165-180

Table 1. FEM simulation phases and activations of Block 37

Stage	Phase	Activation
0	1	Freight tunnel installation
	2	Consolidation
	3	Wall installation
	4	Resetting displacements
	5	Potholing
	6	Refilling
1	7	Dewatering and excavating to 6.2 m
	8	B1 slab installation
2	9	Dewatering and excavating to 9.8 m
	10	B2 slab installation
3	11	Dewatering and excavating to 12.2 m
	12	B3 slab installation
4	13	Dewatering and excavating to 15 m
	14	B4 slab installation

The lateral support was provided by reinforced concrete slabs which were attached to the wall with a moment-resisting connection. Thus, the slabs might pull the wall into the excavation after they were poured due to shrinkage or creep of the concrete since these slabs were firmly connected to the wall as soon as they were placed. Consequently, the deformation recorded at stage 1 was more likely to represent that which was induced by the excavation than those at the other stages since shrinkage or creep of the concrete was likely to induce additional deformations during the excavation process.

CALIBRATION OF SOIL MODEL

Inverse Analysis of Triaxial Data

To optimise the parameters for the triaxial test results, the principal stress differences and excess pore water pressures versus the axial strain were selected as observations for the undrained tests, while the principal stress differences and volumetric strain versus the axial strain were chosen as observations for the drained tests. The number of points that served as observations varied depending on the strain to failure and the model type. For the HSS model, the curves were discretised for the inverse analysis by considering one observation point every 0.005% of the axial strain between 0.001-0.1%, every 0.05% between 0.1-1%, and every 0.5% between 1% and failure strain. Only the data where axial strains were larger than 0.5% were used to optimise the HS parameters because the model does not have the capability to replicate very small strain behaviour. Because of the different numbers of data points used for the various tests, the computed objective function in equation (1) was normalised by the number of data points used in each optimisation (F'(b)) as a means to easily evaluate the relative fit.

The values of the HS parameters used to start the optimisation were those found by Calvello [11], based on the field performance of a Chicago State excavation project located approximately 1 km from Block 37 site. In addition to these same initial parameters, G_0^{ref} was calculated by equations (3) and (4), and $\gamma_{0.7}$ was set at 0.001%.

Maejo Int. J. Sci. Technol. **2015**, *9*(02), 165-180

To illustrate the best fits obtained from the optimisation, Figure 7 shows the computed and measured stress-strain responses of the undrained TC and RTE tests and the drained CMS and CMSE tests of the Blodgett specimens at a conventional scale. The computed results are those based on the optimised parameters of the HSS model for each test. Also shown next to each curve are the values of the normalised objective function, F'(b). The HSS model is found to be limited in its capacity to represent the responses of excess pore pressure in the RTE tests, given the poor fit and large F'(b) value. In contrast, the other results are well represented by the HSS model using the optimised parameters. The results of simulations for specimens from the other two strata also exhibit the same trends.

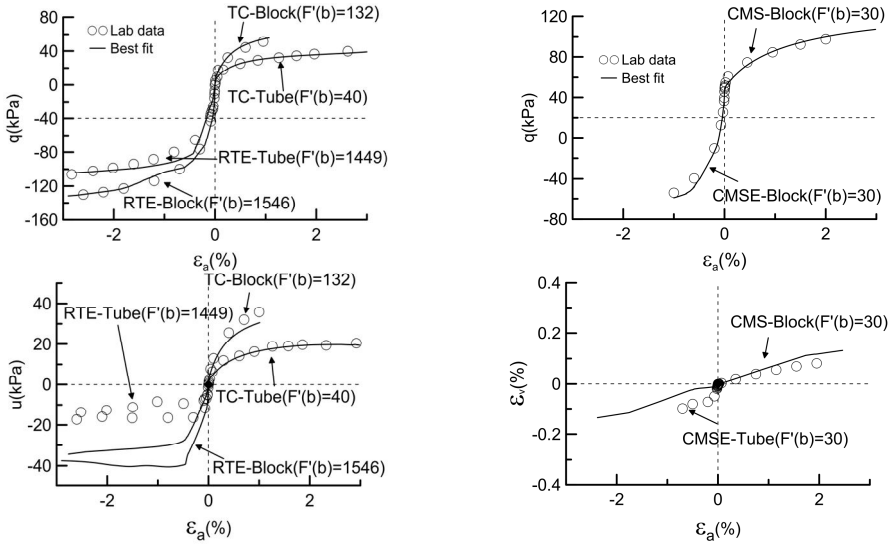

Figure 7. Comparison of best fit responses to laboratory responses of triaxial test for Blodgett specimens: (a) q-ε_a and u-ε_a curves of undrained TC and RTE; (b) q-ε_a and ε_v-ε_a curves of drained CMS and CMSE

To better illustrate the small strain variations, Figure 8 shows the results of the same tests in Figure 7, but they are plotted as normalised secant shear stiffness versus the log of shear strain. The shear strain is defined as $2(\varepsilon_a - \varepsilon_r)/3$, where ε_a is the axial strain and ε_r is the radial strain. The secant shear stiffness is normalised by the G_0 value determined from the bender element tests performed at the end of consolidation and from the drained creep in each test. As indicated in Figure 8, the initial stiffness based on the on-specimen instrumentation from the extension tests was larger than that from the triaxial compression tests. The initial stiffness of the extension tests was much closer to that measured from the bender elements, which is consistent with the results reported in many references [20-22]. Kung et al. [21] and Finno and Cho [22] indicated that the smaller values in the compression results are likely to arise from insufficient strain accuracy of capturing the elastic behaviour of the soil. Note that the differences in the maximum values of G_{sec}/G_0 between those measured from extension tests and compression tests using block samples were smaller than those based on the tube sample results. This result is a direct measure of the better sample quality obtained from the blocks when compared to the tube samples.

Maejo Int. J. Sci. Technol. **2015**, *9*(02), 165-180

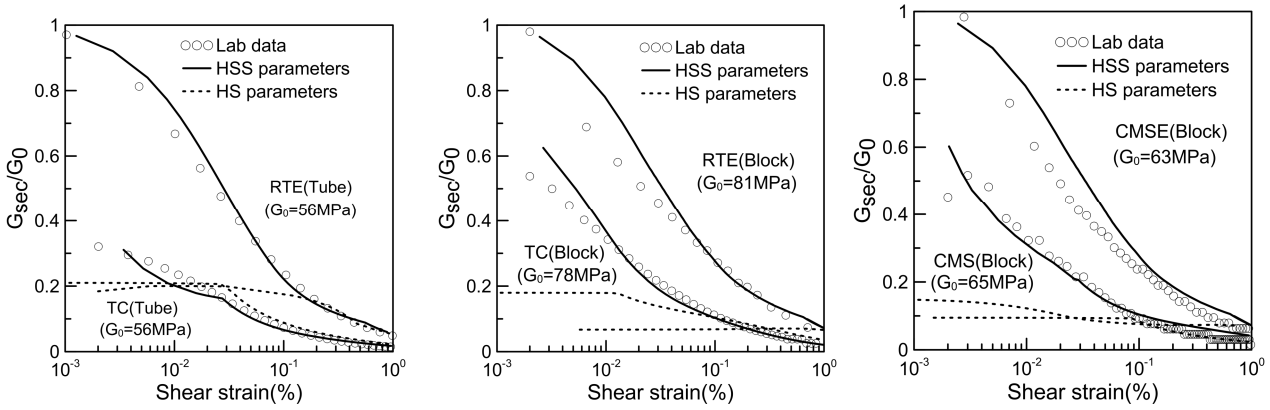

Figure 8. Comparison of computed (with optimised parameters) and measured stiffness-strain responses at small strain level for Blodgett specimens: (a) TC and RTE (tube sample); (b) TC and RTE (block sample); (c) CMS and CMSE

In the TC (block) test the soil stiffness at the small strain level was closer to that in the field than that based on the TC (tube) results; the value of $\gamma_{0.7}$ based on RTE tests for Chicago clay [15] was found to be in the order of 0.01% while $\gamma_{0.7}$ was smaller than 0.001% in the TC tests. This latter value could not be measured in the laboratory using the internal instrumentation used in this study. In any case, after optimisation, the HSS model can represent the responses reasonably well. Table 2 summar-

Table 2. Optimised HSS and HS parameters for triaxial tests

Sample	Test	HSS model					HS model		
		ψ	$E_{50}^{ref}(kPa)$	$\gamma_{0.7}$	$F'(b)$	$\gamma_{0.7}(Lab)^2$	ψ	$E_{50}^{ref}(kPa)$	$F'(b)$
Blodgett Tube	TC	1	8700	4.21E-06	40	<1.00E-6	0.2	7900	230
	RTE	10	3600	7.32E-05	1449	7.00E-5	13	3800	2102
Blodgett Block	TC	0.2	7800	1.21E-05	132	<1.00E-6	0.1	8600	423
	RTE	2.3	3600	7.56E-05	1546	7.00E-5	6	3200	1870
	CMS	0.8	5900	2.48E-05	30	<1.00E-6	0	5100	100
	CMSE	0.1	2900	3.97E-05	30	8.00E-5	1	3200	121
	CQU	1.2	4000	1.13E-04	1025	-	7	7600	46
Deerfield Tube	TC	3.4	10800	3.70E-06	41	<1.00E-6	2.5	14000	131
	RTE	0.4	3000	6.74E-05	374	8.00E-5	20	3400	2456
Deerfield Block	TC	0.1	7800	1.36E-05	142	1.00E-6	0.1	11000	170
	RTE	0.4	3400	5.82E-05	3715	1.00E-4	1	3800	4121
	CMS	0.5	5400	1.35E-05	55	3.00E-6	0	11000	111
	CMSE	0.7	3300	7.84E-05	36	1.00E-4	0.1	3200	143
	CQU	0.7	1900	2.34E-04	7271	-	-	-	-
Park Ridge Tube	TC	0.8	8500	5.91E-06	47	<1.00E-6	2.6	5600	67
	RTE	9	4000	7.40E-05	2582	8.00E-5	10	4300	4234

Note: 1) p^{ref}=100 kPa; 2) $\gamma_{0.7}$(Lab) refers to $\gamma_{0.7}$ estimated from laboratory tests.

ises the values of the optimised HSS and HS parameters and the normalised objective function values for each of the triaxial tests. As presented in Figure 7 and Table 2, an F'(b) value smaller than approximately 150 indicates a reasonable fit. As illustrated with the Blodgett data, the HSS model, even using optimised parameters, cannot represent the soil behaviour in the RTE and CQU modes of shearing for any of the specimens (F'(b)>1000).

It can be recalled that the three individual parameters, E_{50}^{ref}, Ψ and $\gamma_{0.7}$, were optimised for each triaxial result. The values of Ψ are usually smaller than 1, which is consistent with the Chicago clay being lightly overconsolidated. Exceptions include the RTE data for the Blodgett (tube sample) and the Park Ridge specimens. The overestimation of Ψ in the RTE tests arises from the poor fit of the excess pore pressures.

The values of E_{50}^{ref} from the TC tests are similar to Cavello's results [11], based on drained TC tests. These values are approximately 2 to 3 times the value of E_{50}^{ref} determined from the extension tests. The reason for this apparent discrepancy is illustrated in Figure 9, which shows the computed stress-strain results from the simulations of the TC and RTE tests following two pre-shear stress paths, K_0 consolidation (K_0) and isotropic consolidation (I). The optimised parameters from the TC (block) Blodgett specimen were used for all four simulations, as shown in Figure 9. Normally, in the HS and HSS models, E_{50}^{ref} is defined based on isotropically consolidated drained TC tests. After isotropic consolidation, E_{50}^{ref} is used to calculate the soil responses in both I-TC and I-RTE test simulations because both paths are "loading" paths. One can note the same value of stiffness in both modes of shear for the isotropic consolidation results. In contrast, after K_0 consolidation, whereas E_{50}^{ref} is used to calculate the soil response in a K_0-TC (loading) path, E_{ur}^{ref} is used to calculate the soil response in the K_0-RTE (unloading) path. When optimising parameters based on the K_0-RTE test results, E_{ur}^{ref}, defined as $3E_{50}^{ref}$, is really the operative stiffness because of the unloading in the test. Thus, the optimised E_{50}^{ref} based on the analysed extension tests should be one-third of the E_{50}^{ref} from the compression tests. The optimized E_{50}^{ref} values from the extension tests presented in Table 2 generally are one-half to one-third of those based on the compression tests. Thus, one should not use extension tests to find the E_{50}^{ref} values using this optimisation method.

A comparison between the optimised and observed $\gamma_{0.7}$ values is also presented in Table 2. The values of $\gamma_{0.7}$ obtained from inverse analysis are similar to the experimental $\gamma_{0.7}$ values for the extension tests, which provided the entire modulus reduction curve. The $\gamma_{0.7}$ values for the TC tests cannot be extracted from the data in Figure 8, but those obtained from the inverse analysis suggest that they are smaller than 0.0001%, which, again, is too small to be measured with the internal instrumentation. This trend arises because the G_0 parameters in the HSS model were taken from bender element results rather than the maximum value of shear stiffness from the internal instrumentation. Because the HSS model does not allow for a different value of $\gamma_{0.7}$ based on the direction of loading or, more specifically, based on recent stress history [22], this type of response was not replicated in the model.

Maejo Int. J. Sci. Technol. **2015**, *9*(02), 165-180

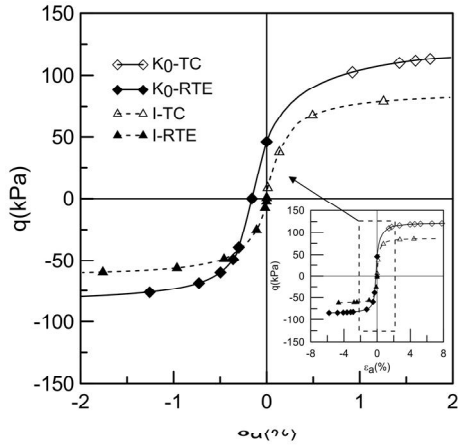

Figure 9. Plot of q versus ε_a: simulations of the TC and RTE tests using Blodgett TC (block) parameters in Table 2

Finally, as presented in Table 2, the optimised values of E_{50}^{ref} are not the same for the HS and HSS models. Apparently, one should use caution if the HS-based stiffness values are used directly with the two small strain parameters in the HSS model.

Inverse Analysis of Braced Excavation

Table 1 summarises the simulation phases in Plaxis defined to represent the major construction activities during the excavation of Block 37. Details of the simulation can be found in the work of Kern [17]. An interface was modelled between the wall and the soil. Freight tunnel construction (see Figure 2) and potholing were simulated to reflect the effects of these activities on the soil stresses before excavation began. Unfortunately, it was difficult to simulate the potholing properly when the potholes were excavated in the field to unknown dimensions. Site photographs provided approximate dimensions of these activities along the north wall. To minimise the errors related to the potholing simulation and the shrinkage and creep of concrete in the floor slab that provided lateral support, the incremental deformation induced by excavation at stage 1 was used as observations in the inverse analysis to optimise the soil parameters. Herein, the incremental deformation at stage 1 minus the deformation measured at the potholing stage was defined as deformation at stage 1'. The inclinometer data obtained within the Blodgett, Deerfield and Park Ridge layers were used to optimise the parameters for those deposits.

The Blodgett, Deerfield and Park Ridge layers were modelled as both HS and HSS materials, and the remaining strata were modelled as HS materials. The soil stiffness parameters E_{50}^{ref} and $\gamma_{0.7}$ were optimised in the inverse analysis of the excavation. The initial small strain parameters, $\gamma_{0.7}$, for each layer were estimated based on the inverse analysis of laboratory tests with the lowest value of F'(b).

Figure 10 illustrates a comparison of the computed deformations and the observed deformations, where the former are based on the optimised HSS and HS parameters. As expected, the computed deformations based on the optimised parameters agree well with the measured deformations at the first stage. The optimised HSS and HS parameters are used to compute the wall deformations at the final ex-

Maejo Int. J. Sci. Technol. **2015**, *9*(02), 165-180

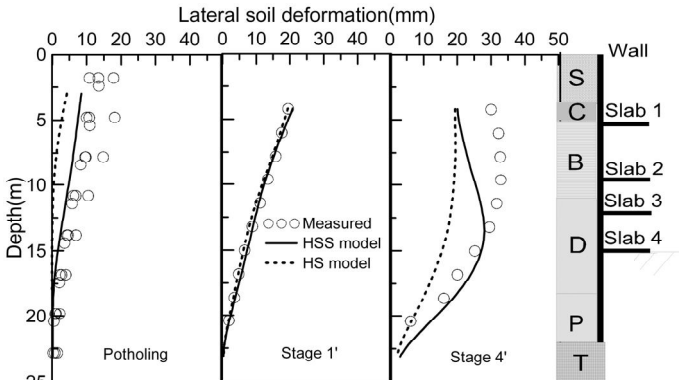

Figure 10. Comparison of computed and measured lateral soil deformations using optimised parameters

cavation stage. Figure 10 also shows that the computed wall deformations at the final excavation stage using optimised HSS parameters are as much as 10 mm smaller than the measured deformations above the bottom of the excavation. However, below the bottom of the excavation, the computed deformations are much more consistent with the measured ones. This discrepancy is likely to be due to the shrinkage and creep of the concrete slab, which was not considered in the simulation of the excavation [17]. The calculated wall deformation using the HS model is smaller than the measured deformation both below and above the bottom of the excavation because the stiffness of the soil was overestimated to fit the deformation at the first stage when the deformations were relatively small and the ground strains were very small. The advantage of using a model with small strains is clear because of its capabilities to allow for use of the appropriate stiffness for a wider range of strains.

Table 3 presents the optimised parameters based on the inclinometer data from the excavation at stage 1'. The values of E_{50}^{ref} optimised from the inclinometer data using the HSS model are close to those optimised based on undrained TC results of the block samples of the Blodgett and Deerfield strata. The optimised E_{50}^{ref} values for the HS model are larger than those for the HSS model. This difference is expected when the deformation is relatively small because the full range of stiffness is not considered in the HS model and a higher value is required to result in a smaller deformation.

Table 3. Optimised parameters for HSS and HS models based on data from excavation

	HSS model		HS model
	E_{50}^{ref} (kPa)	$\gamma_{0.7}$	E_{50}^{ref} (kPa)
Blodgett	8200	7.64×10^{-5}	10000
Deerfield	7600	6.56×10^{-5}	14000
Park Ridge	12700	7.21×10^{-5}	32000

Note: p^{ref} = 100 kPa

Maejo Int. J. Sci. Technol. **2015**, *9*(02), 165-180

The optimised values of $\gamma_{0.7}$ are close to those optimised based on the extension tests. The reasons for this similarity might be the insufficient strain accuracy to capture the elastic behaviour of soil in compression tests [21, 22] and also the chance that the soil in front the retaining wall, which was subjected to extension, may dominate the lateral wall deformation. Usually, when the properties of a laboratory sample are more similar to those of the sample in the field, a better sample quality is indicated. It can be recalled that the only difference between TC (block) and TC (tube) is the quality of the sample, while $\gamma_{0.7}$ from TC (block) is closer to $\gamma_{0.7}$ obtained from the *in situ* data, which indicates that the quality of the block sample is better than that of the tube sample. Figure 11 indicates that the soil deformations are strongly influenced by $\gamma_{0.7}$: the deformations decrease when $\gamma_{0.7}$ increases. Therefore, the small strain behaviour of the soil surrounding the excavation must be considered when one calculates soil deformations induced by the excavation.

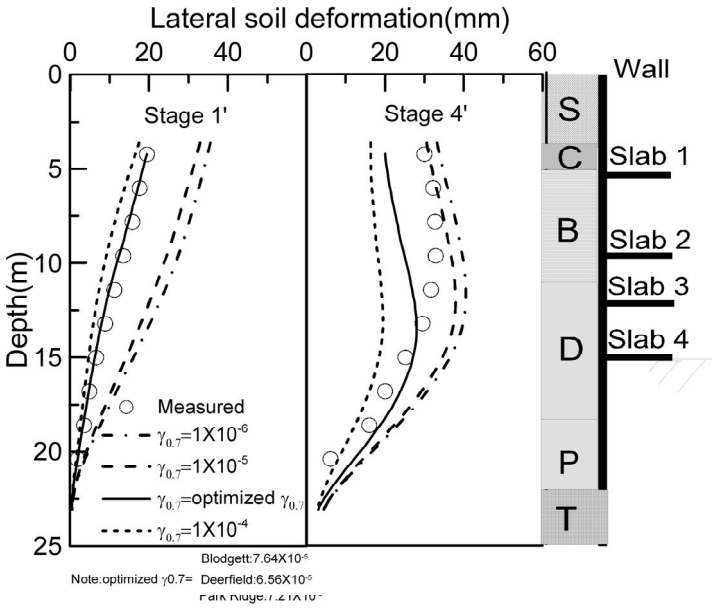

Figure 11. Computed lateral soil movement induced by excavation using different $\gamma_{0.7}$ values

CONCLUSIONS

Based on the results of the laboratory experiments, field observations and numerical simulations for the excavation of Block 37 through compressible Chicago glacial clays, the following conclusions can be drawn:

(1) The HS and HSS models cannot describe the soil responses following different stress paths using a unique set of soil parameters. In particular, neither model can simulate the stress-strain responses from the CQU tests or the excess pore pressure responses of the RTE tests. In general, with the use of proper parameters, the HSS model better represents the soil responses than does the HS model, both in the field and in the laboratory, especially at relatively small strain levels.

(2) The values of $\gamma_{0.7}$ optimised based on TC (block), compared with $\gamma_{0.7}$ optimised based on TC (tube), are closer to those optimised based on the *in situ* data, which reflects the higher quality of the block samples compared to the tube samples.

(3) The soil stiffness at small strain levels significantly influences the soil deformations induced by

Maejo Int. J. Sci. Technol. **2015**, *9*(02), 165-180

excavation, at least for the deformation levels encountered at Block 37 site, which is consistent with the observations of other researchers regarding the importance of small strain non-linearity.

(4) For the HSS and HS models, the values of E_{50}^{ref} optimised based on field performance data produce similar results to those obtained from the optimisation based on the TC results from block specimens. For the HSS model, $\gamma_{0.7}$ optimised based on performance data produces similar results to those obtained from $\gamma_{0.7}$ optimised based on RTE results.

(5) The optimised values of E_{50}^{ref} for the same stress path in the laboratory are not the same for the HS and HSS models. One should not use stiffness parameters derived from the HS model in the HSS model without evaluating the computed responses in light of the effects of the two small strain parameters

ACKNOWLEDGMENTS

The financial support for this work was provided by the National Science Fund of China through Grant No. 51208378 and by the National Science Foundation of USA through Grant No. CMMI-0928184.

REFERENCES

1. B. Simpson, N. J. O'Riordan and D. D. Croft, "A computer model for the analysis of ground movements in London clay", *Géotechnique*, **1979**, *29*, 149-175.
2. J. B. Burland, "The stiffness of soils at small strain", *Can. Geotech. J.*, **1989**, *26*, 499-516.
3. A. J. Whittle, Y. M. A. Hashash and R. V. Whitman, "Analysis of deep excavation in Boston", *J. Geotech. Eng.*, **1993**, *119*, 69-90.
4. S. E. Stallebras and R. N. Taylor, "The development and evaluation of a constitutive model for the prediction of ground movements in overconsolidated clay", *Géotechnique*, **1997**, *47*, 235-253.
5. L. C. Jen, "The design and performance of deep excavations in clay", *PhD Thesis*, **1998**, Massachusetts Institute of Technology, USA.
6. R. J. Finno, I. S. Harahap and P. J. Sabatini, "Analysis of braced excavations with coupled finite element formulations", *Comput. Geotech.*, **1991**, *12*, 91-114.
7. C. W. W. Ng, "Stress paths in relation to deep excavations", *J. Geotech. Geoenviron. Eng.*, **1999**, *125*, 357-363.
8. Y. M. A. Hashash and A. J. Whittle, "Mechanisms of load transfer and arching for braced excavations in clay", *J. Geotech. Geoenviron. Eng.*, **2002**, *128*, 187-197.
9. C. Rechea, S. Levasseur and R. J. Finno, "Inverse analysis techniques for parameter identification in simulation of excavation support systems", *Comput. Geotech.*, **2008**, *35*, 331-345.
10. R. J. Finno and M. Calvello, "Supported excavations: Observational method and inverse modeling", *J. Geotech. Geoenviron. Eng.*, **2005**, *131*, 826-836.
11. M. Calvello, "Inverse analysis of a supported excavation through Chicago glacial clays", *PhD Thesis*, **2002**, Northwestern University, USA.
12. T. Schanz, P. A. Vermeer and P. G. Bonnier, "The hardening soil model--formulation and verification", Proceedings of Plaxis Symposium--Beyond 2000 on Computational Geotechnics, **1999**, Amsterdam, Netherlands, pp.281-296.

Maejo Int. J. Sci. Technol. **2015**, *9*(02), 165-180

13. T. Benz, R. Schwab and P. Vermeer, "Small-strain stiffness in geotechnical analyses", *Bautechnik*, **2009**, *86*, 16-27.
14. J. F. Labuz and A. Zang, "Mohr-Coulomb failure criterion", *Rock Mech. Rock Eng.*, **2012**, *45*, 975-979.
15. T. Kim, "Incrementally nonlinear responses of soft Chicago glacial clays", *PhD Thesis*, **2011**, Northwestern University, USA.
16. M. Calvello and R. J. Finno, "Selecting parameters to optimize in model calibration by inverse analysis", *Comput. Geotech.*, **2004**, *31*, 410-424.
17. K. Kern, "Analysis of pseudo top-down construction in Chicago", *Master Thesis*, **2011**, Northwestern University, USA.
18. R. J. Finno and C. K. Chung, "Stress-strain-strength responses of compressible Chicago glacial clays", *J. Geotech. Eng.*, **1992**, *118*, 1607-1625.
19. J. H. Atkinson, D. Richardson and S. E. Stallebrass, "Effect of recent stress history on the stiffness of overconsolidated soil", *Géotechnique*, **1990,** *40*, 531-540.
20. R. J. Jardine, "Some observations on the kinematic nature of soil stiffness", *Soils Found.*, **1992**, *32*, 111-124.
21. G. T. C. Kung, C. Y. Ou and C. H. Juang, "Modeling small-strain behavior of Taipei clays for finite element analysis of braced excavations", *Comput. Geotech.*, **2009**, *36*, 304-319.
22. R. J. Finno and W. J. Cho, "Recent stress-history effects on compressible Chicago glacial clays", *J. Geotech. Geoenviron. Eng.*, **2011**, *137*, 197-207.